Evaluation of Thermal Stress in Airport Concrete Pavement Slab by 3D-FEM Analysis

<Taizo SHIMOMURA[1], Tatsuo NISHIZAWA[2] and Takato OZEKI[3]>

Abstract

Thermal stress caused by temperature distribution in pavement slab is important in the structural design of airport concrete pavements. Airport concrete pavement slab is very thick, therefore, temperature in the pavement slab varies nonlinearly throughout the slab depth. Thermal stress caused by the nonlinear temperature distribution would be different from that of linear temperature distribution.

In this research, thermal stress in concrete pavement slab has been investigated as follows. 1) Thermal stresses caused by nonlinear temperature distribution were calculated using temperatures and restraint strains measured in an experimental concrete pavement with a 46cm thick slab. 2) 3DFEM model was developed on the experimental concrete pavement and numerical simulations were performed to validate the model by comparing the simulated thermal strains and stresses with the measured ones. 3) The thermal stress in thick concrete pavement slab was discussed based on the 3DFEM simulations in terms of structural design of concrete pavement. From the measurement, it was found that the nonlinearity in temperature distribution strongly affects the magnitude of thermal stress in thick concrete slab. Also, it was confirmed that 3DFEM model is appropriate tool to estimate the thermal stress in thick concrete slabs taking into account the nonlinear temperature distribution.

[1] TAISEI Corporation. Address: 6-8-1 Nishi Shinjuku, Shinjuku-ku, Tokyo 163-6006 JAPAN
E-mail: taizo@ce.taisei.co.jp
[2] Professor, Ishikawa National College of Technology. Address: Tsubata, Ishikawa, 929-0392 JAPAN
E-mail: nishi@ishikawa-nct.ac.jp
[3] TAISEI Corporation. Address: 2-16-33 Hakusan, Midori-ku, Yokohama, Kanagawa 226-0006 JAPAN
E-mail: ozktkt00@pub.taisei.co.jp

1. Introduction

A concrete pavement slab deforms by external environment effects such as rain, wind, solar irradiation, humidity and temperature. However, self-weight and friction force from base course and joint reinforcement restrain the deformation of the concrete slab and the following restraint stresses are generated in the concrete pavement slab.

(1) Long-term thermal stress, which is caused by yearly temperature change.
(2) Shrinkage stress, which is caused by dry shrinkage and autogenous shrinkage.
(3) Thermal stress, which is caused by daily temperature change.

However, thermal stress is the most critical, because its magnitude is greater than the other restraint stresses (long-term thermal stress and shrinkage stress) in Japan. Therefore, the thermal stress is taken into account in the structural design of concrete pavement.

In Japan, the thermal stress in concrete slab has been calculated by Iwama formula (Iwama. 1963), as will be described in later section. This formula was developed by modifying Westergaard formula (Westagaard. 1926) being based on the measuring results on 20 to 25cm thickness road pavement slabs. Iwama formula considers curling stress that is caused by linear temperature distribution throughout concrete slab depth and reduces the stress by 30% considering internal stress, which is caused as the result of nonlinear temperature distribution. However, airport concrete pavement slab is very thick, hence, the internal stress caused by nonlinear temperature distribution would be much larger than that in normal road concrete slab. Therefore, it is expected that actual thermal stress of airport concrete pavement is different from that calculated by Iwama formula.

The purpose of this research is to investigate the thermal stress in thick concrete pavement slab and develop a reasonable method to calculate the actual thermal stress that includes nonlinear component as well as liner component in temperature distribution for the structural design of the airport concrete pavement. For that, temperature and strain measurements in an experimental concrete pavement were conducted over one year. A 3DFEM model was developed to simulate the experimental results and validated by comparing the calculated results with the measured ones. Finally, the effects of the thermal stress in thick concrete slab on the structural design were discussed.

2. Strain and Temperature Measurements in Experimental Concrete Pavement

2.1. Experimental Overview

Strain and temperature measurements were carried out in an experimental concrete pavement as shown in Figure 1. Strain and temperature gauges were embedded in the concrete pavement slabs of Unit C and Unit D. The slab in each unit was 8.5m length, 8.5m wide and 0.46m thick. There were 6 measuring points in each unit. Each measuring point had 3 strain gauges and 6 temperature gauges in the depth direction of the slab to measure strain and temperature distributions.

The composition of the concrete used in Unit C and Unit D are presented in Table 1. The design strength of the concrete was 5.5MPa for Unit C, and 5.0MPa for Unit D. In addition, laboratory tests were carried out to estimate elastic modulus, Poisson’s ratio, and thermal expansion coefficient of the concretes. The results are summarized in Table 2.

These properties were used to calculate the thermal stress from the measured strains and temperatures in the experimental concrete pavement.

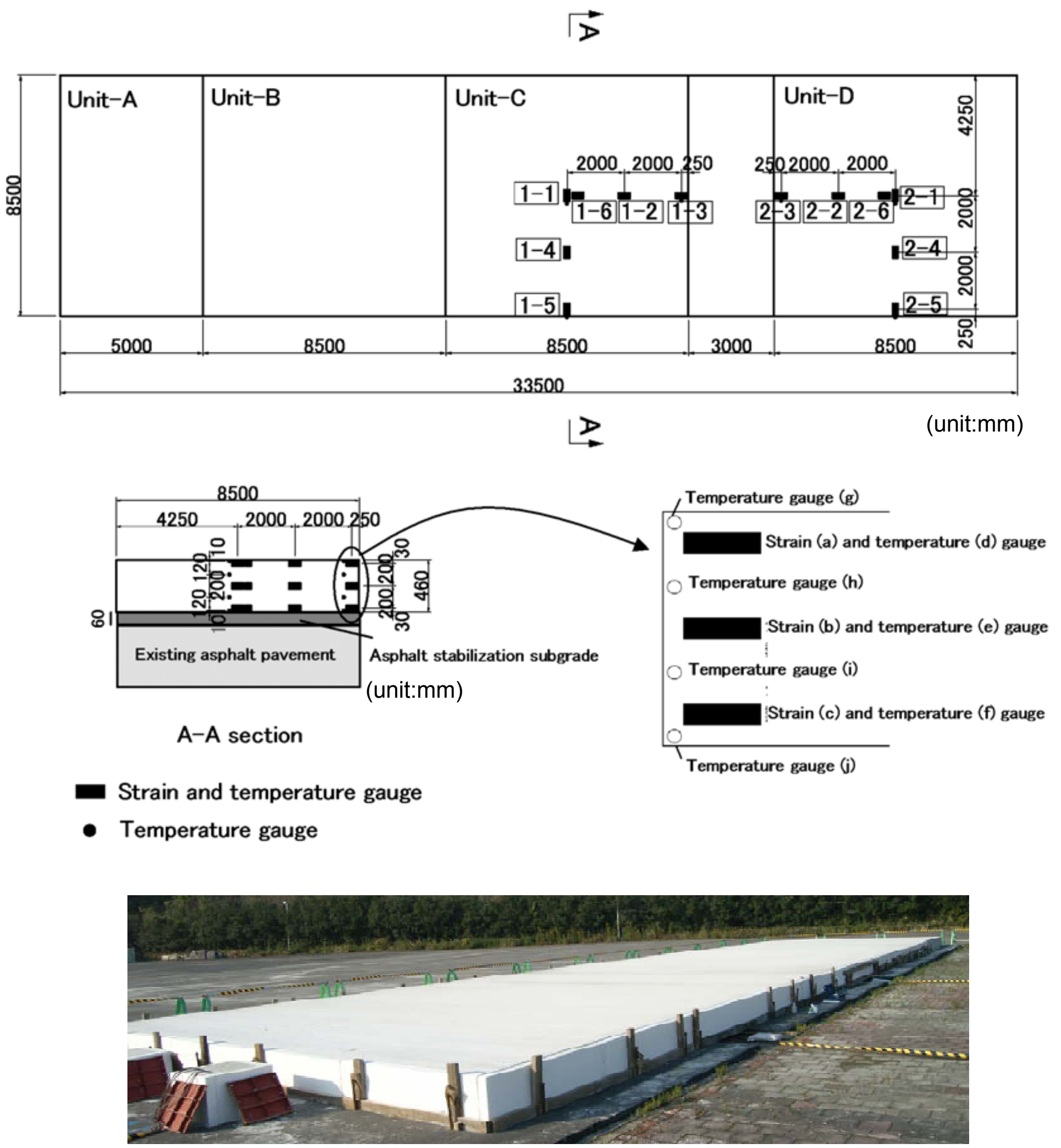

Figure 1 Full scale experimental pavement

Table 1 Compositions of the concretes

	C/W	W/C (%)	Unit coarse aggregate volume	s/a (%)	Unit weight (kg/m^3)					Admixture	
					W	C	S	4020	2005	C□%	Kg/m^3
Unit-C (5.5Mpa)	2.7	37.0	0.76	32.7	134	362	599	511	759	1.0	3.62
Unit-D (5.0Mpa)	2.2	45.5	0.76	35.9	127	279	685	511	759	1.0	2.79

Table 2 Laboratory test results

	Thermal expansion coefficient α (μ /^{o}C)	Elastic Modulus E (N/mm^2)	Poisson's Ratio ν
Unit-C	8.89	39,900	0.206
Unit-D	8.97	41,700	0.204

2.2. Strain and Temperature Measuring Results

Strains and temperatures were continuously measured at all measuring points over a year from October 2006 to September 2007. Variations of measured strain and temperature at the lowest gauges at the central point of Unit C (measuring point: 1-1) are shown in Figure 2. As can be seen in Figure 2, the strain and the temperature changed corresponding with each other during the year.

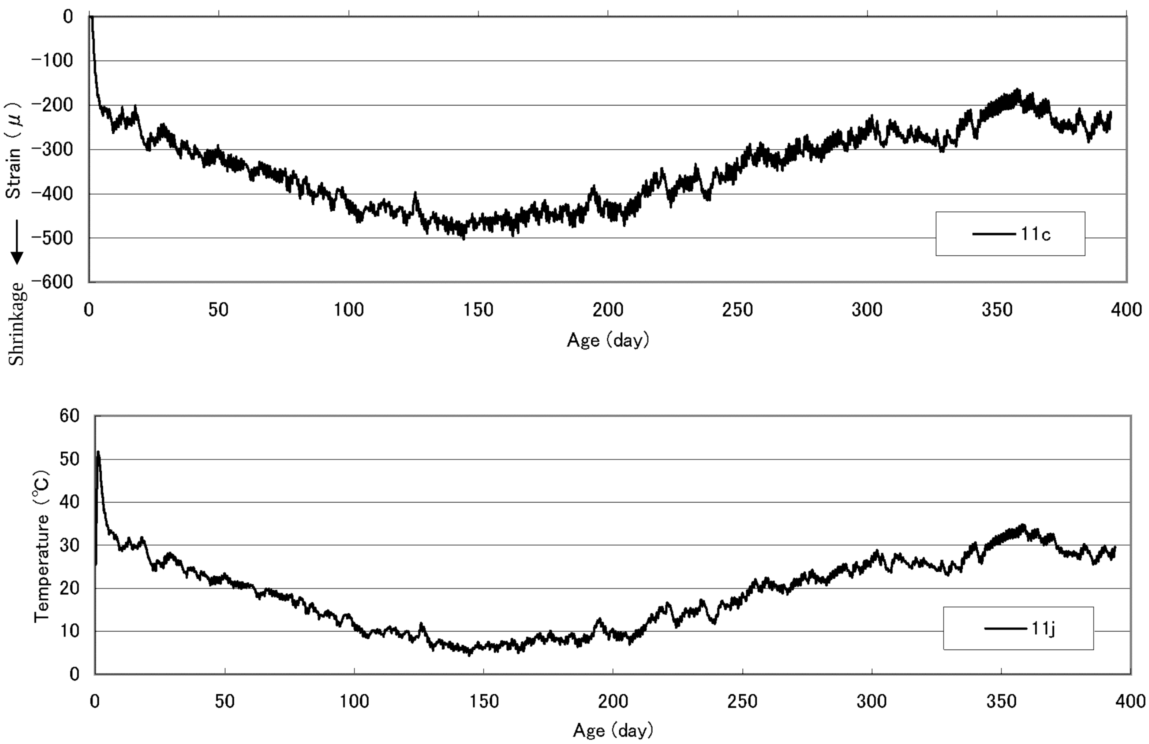

Figure 2 Variations of measured strain and temperature during a year at measuring point 1-1

3. Thermal Stress Calculated from Strain and Temperature Measuring Results

3.1. Thermal stress

Restraint stress caused by temperature in a concrete slab can be divided into three restraint stresses; axial stress, curling stress, and internal stress, as shown in Figure 3. The axial stress is caused by base course or joint restraining axial deformation of the slab due to average temperature change. The curling stress is resulted from restraint of self weight on curling deformation of the slab due to linear component of temperature distribution throughout the slab depth. The internal stress is caused by nonlinear component of temperature distribution.

The axial stress tends to be compressive stress or minuscule tensile stress. Therefore, it is supposed to be conservative to neglect the stress in the current structural design procedure (Iwama. 1963). Hence, the axial stress was excluded and the thermal stress, which is a summation of the curling stress and the internal stress, was discussed in this research.

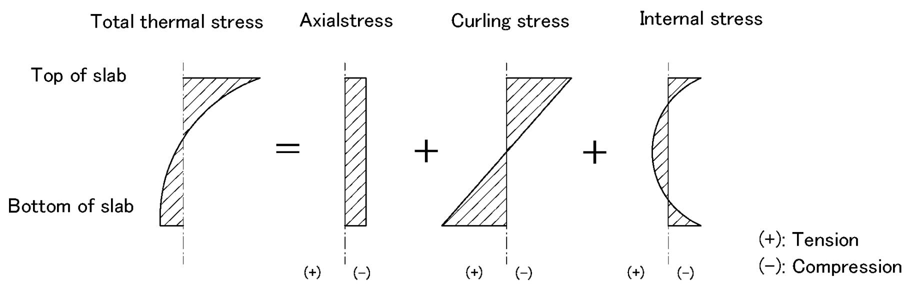

Figure 3 Restraint stress caused by temperature in concrete slab

3.2. Procedure of Calculating Thermal Stress Based on Measuring Results

The measured strains and temperatures are divided into axial (average) component, curling (linear) component, and internal (nonlinear) component (Nishizawa et al. 1998), as illustrated in figure 4. Restraint strain can be obtained by subtracting temperature strain from measured strain. This operation can be performed assuming the following expression:

$$f(z) = a + \beta \cdot z + g(z) \tag{1}$$

where, $f(z)$: distribution of the strain and temperature throughout the slab depth, a: average component, β: gradient of linear component, and $g(z)$: nonlinear component.

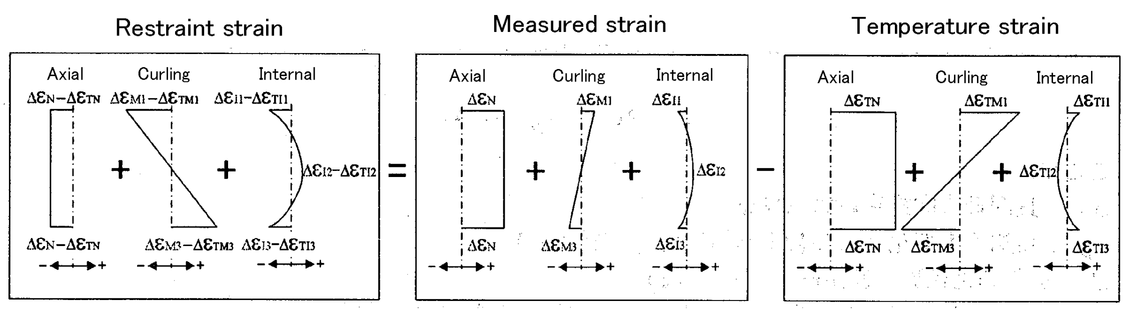

Figure 4 Procedure of dividing measured responses into three components.

In this research, a quadratic approximation is employed for *g(z)* as:

$$g(z) = b_0 + b_1 z + b_2 z^2 \tag{2}$$

were, b_i are constants that can be determined from measured data at top, middle and bottom of concrete slab at each time of day in terms of increment of the measured response from a standard time. The standard time is defined as the time when the temperature difference between the top and bottom of the slab is the minimum on each day. The assumption of the quadratic expression of temperature and strain through depth of concrete slab can be proved to be valid from Figure 5, showing that approximated temperature and strain distributions by the quadratic equation are very close to the measured ones at each time of day. Also, the figure reveals that the distributions of strain and temperature have nonlinearity.

Assuming one dimensional stress state, the thermal stress can be calculated by:

$$\sigma_T = E_c(\varepsilon - \varepsilon_T) = E_c(\varepsilon - \alpha T) \qquad (3)$$

where, σ_T : the thermal stress, α : thermal expansion coefficient, E_c : elastic modulus of concrete, ε : measured total strain, and ε_T : temperature strain.

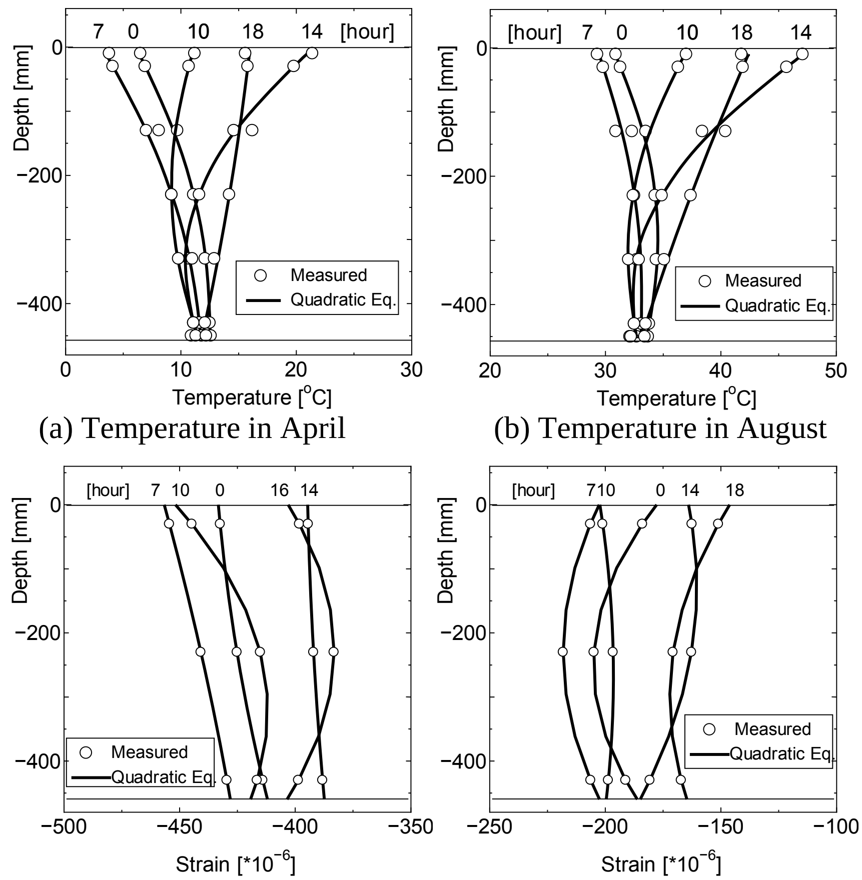

(a) Temperature in April (b) Temperature in August

(c) Strain in April (d) Strain in August

Figure 5 Quadratic approximation of temperature and strain distribution in concrete slab

3.3. Calculating Results of Thermal Stress

According to the procedure as described in 3.2., the thermal stress at each measuring points in the concrete pavement slabs was calculated. The thermal stress at the bottom of the pavement slab will be focused in this section, because large tensile stress at the bottom of slab is generated by aircraft loads and combined stress that is a summation of thermal stress and loading stress is considered in the structural design in Japan. Figure 6 shows variations of the thermal stresses at the bottom of the pavement slabs in a day at each central measuring point in Unit C and Unit D (1-6 in Unit C and 2-6 in Unit D) on 15th August. The maximum tensile thermal stress is 1.4 MPa in Unit-C, and 1.5 MPa in Unit-D at central point of the pavement, indicating that there is no difference of the thermal stress due to the compositions of the concretes.

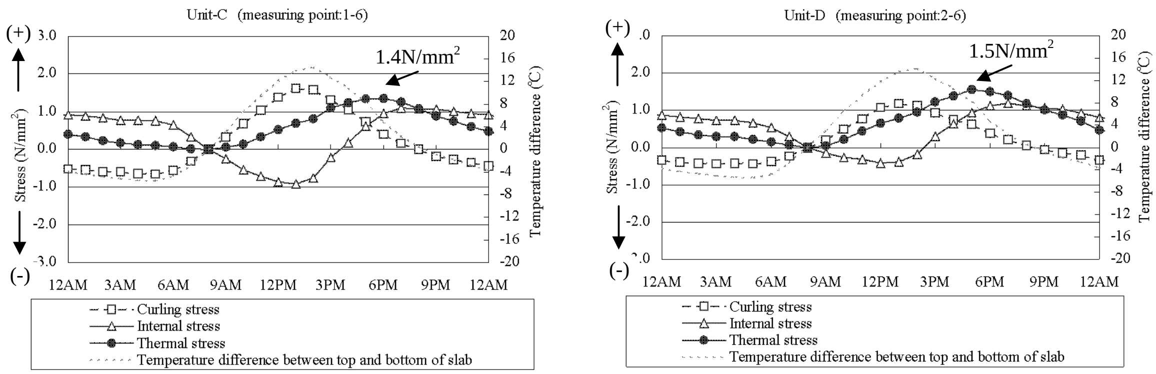

(+): Tension, (-): Compression

Figure 6 Thermal stress at central point (measuring point: 1-6, 2-6) in August

The linear component of thermal stress varies corresponding to the variation of temperature difference, while the nonlinear component varies opposite to the variation of temperature difference. Therefore the variation of the total thermal stress is a little sifted from that of temperature difference and the peak of the tensile stress appears about 4 hours later than that of temperature difference. The maximum tensile stress of linear component is greater than the total thermal stress. It means that the thermal stress estimated only from the linear component would be overestimated. This finding has been stated by many researchers (Harik et al. 1994) (Choubane et al. 1995) (William et al. 2001). In Japan, Iwama investigated the thermal stress on full scale test pavements and suggested that the actual thermal stress should be estimated by reducing 30 % from Westargaard equation. The proposed equation is:

$$\sigma_T = 0.7 \cdot \frac{\alpha \cdot E_c \cdot \theta}{2(1-\nu)} \qquad (4)$$

where, θ: temperature difference between top and bottom of slab (℃), and ν : Poisson's ratio. In this equation, the term, $\alpha \cdot E_{c} \cdot \theta / (2(1-\upsilon))$, is the curling stress suggested by Westagaard, assuming linear temperature distribution and full restraint of slab. Tsubokawa et al. proposed a thermal stress equation based on temperature and strain measurements in 42 cm thick concrete pavement, which accounts for the peak shift of the thermal stress variation (Tsubokawa et al. 2006).

Figure 7 compares the thermal stress calculated by Eq. (4) with the one estimated from the measured temperatures and strains. The difference between two thermal stresses is apparent. The thermal stress by Eq. (4) still overestimates the measured ones, even though the equation is accounting for the nonlinear component. Also, the time of the occurrence of the maximum tensile stress by Eq. (4) is 4 hours earlier than the measured one. Eq. (4) calculates the maximum tensile thermal stress, 2.3 MPa, which is about 50% larger than the measured one: 1.4 MPa for unit-C, and 1.5 MPa for unit-D. This discrepancy might come from the fact that Eq. (4) was developed being based on the experimental examinations on 20-25cm-thickness concrete pavement slabs (Iwama.

1963). Eq (4) proposed by Iwama is only an approximation and this coefficient (=0.7) is dependent on the time of day and level of nonlinearity in the temperature profile. The nonlinearity in temperature distribution in those comparatively thin concrete slabs would be different from thick concrete slabs. Therefore, another method of predicting the thermal stress should be developed for thick concrete slabs in airport pavements.

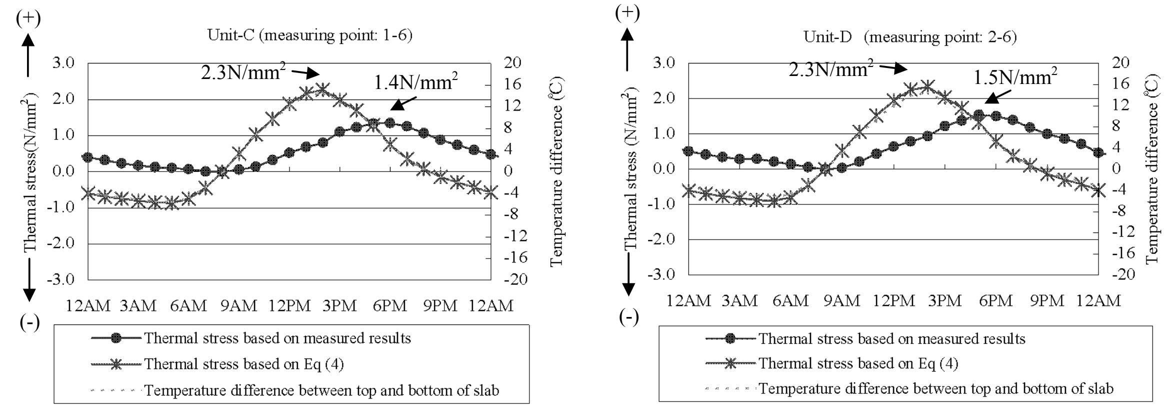

(+): Tension, (-): Compression

Figure 7 Comparative result of thermal stress

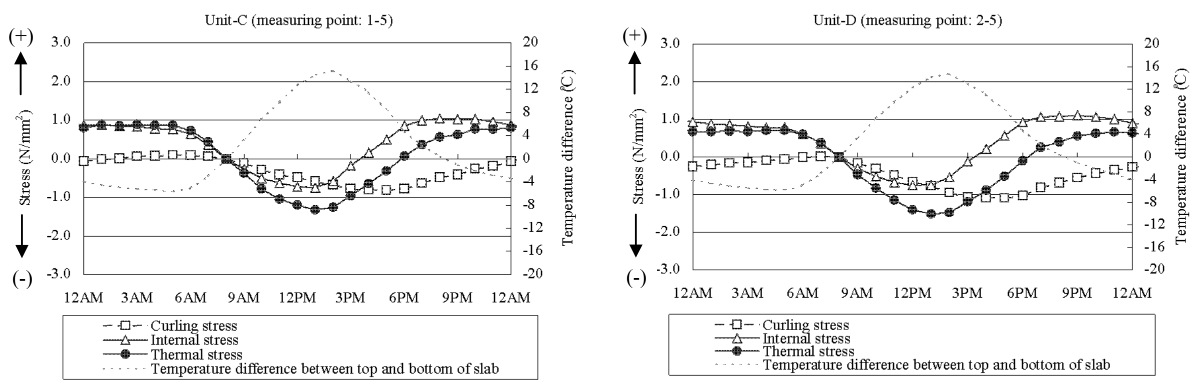

(+): Tension, (-): Compression

Figure 8 Thermal stress at free edge of slab (measuring point: 1-5, 2-5) in August

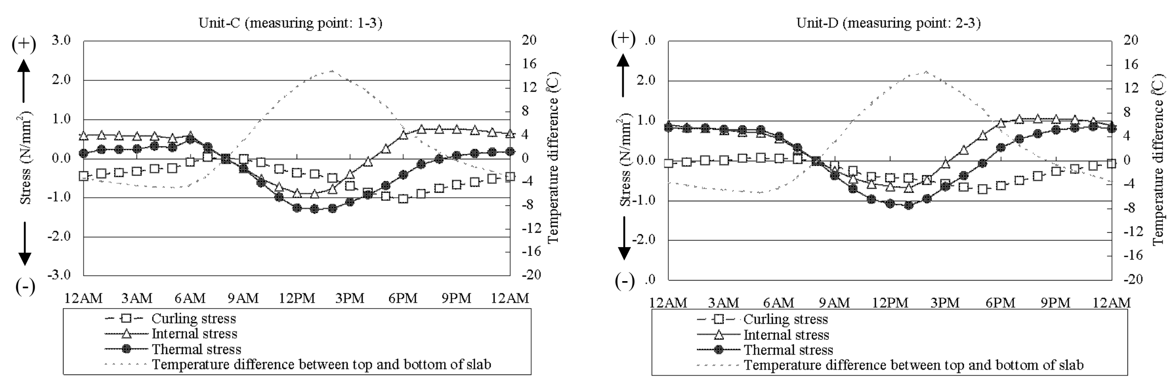

(+): Tension, (-): Compression

Figure 9 Thermal stress at joint edge (measuring point: 1-3, 2-3) in August

Figures 8 and 9 show the variations of the thermal stress at the bottom of the pavement slab in a day at each free edge of the slabs, Unit C and Unit D (measuring points: 1-5 and 2-5) and joint edge of the slabs (measuring point: 1-3 and 2-3) on 15th August.

The thermal stress components in the figures are the ones in the direction perpendicular to the direction of the slab edge. Therefore, the variations of the stress components are quite different from those at the center of the slabs. Since there is little difference in the stresses between at the free edge and joint edge, it can be said that the effect of dowels in the joints is very small and can be neglected in this research.

4. Thermal Stress Calculated by 3D-FEM Analysis

4.1. Formulation of thermal stress

Thermal stress can be calculated by

$$\{\sigma\} = [D](\{\varepsilon\} - \{\varepsilon_T\}) = [D]\{\varepsilon_C\} \qquad (5)$$

where, $\{\sigma\}$:stress vector, $[D]$:elastic matrix, $\{\varepsilon\}$:total strain vector, and $\{\varepsilon_T\}$:thermal strain vector. In three dimensional space, the thermal strain is:

$$\{\varepsilon_T\} = \{\alpha T \quad \alpha T \quad \alpha T \quad 0 \;\; 0 \;\; 0\} \qquad (6)$$

where, T is the temperature and is assumed to be a quadratic function of z as explained in the previous section.

Resent years, complicated mechanical behavior of concrete pavements including thermal stresses were simulated with three dimensional finite element method (3DFEM) utilizing commercially available software packages (William et al. 2001) (Pane et al. 1998) (Shoukry et al. 2003) (Mahboub et al. 2004). In this research, a 3DFEM program, Pave3D, is employed, which has been developed for the structural analysis of pavement structures and is has a feature of dealing with the thermal behaviors of pavement layers (Nishizawa et al. 2005).

4.2. 3DFEM model

3DFEM model used in this research has an 8.5 m by 8.5 m concrete slab with a thickness of 46 cm resting on a 21 cm thick asphalt layer and a 40 cm thick granular base as shown in Figure 10. In the model, each pavement layer is divided into 8 node solid elements. Interface between the concrete slab and asphalt base course is modeled by an interface element that represents the interaction between the slab and base with three linear springs and accounts for the separation when the slab curls up. Considering the symmetry of the structure, a quarter region of the pavement is meshed. The material properties of each layer are summarized in Table 3. The asphalt layer, granular base and subgrade were assumed elastic bodies with elastic moduli as presented in Table 3.

Temperature distribution expressed by the quadratic equation at each time of a day was input into the 3DFEM model and thermal stresses at the time were calculated. The FEM computation was repeated for each time of day of temperature measurement to simulate daily thermal stress variation.

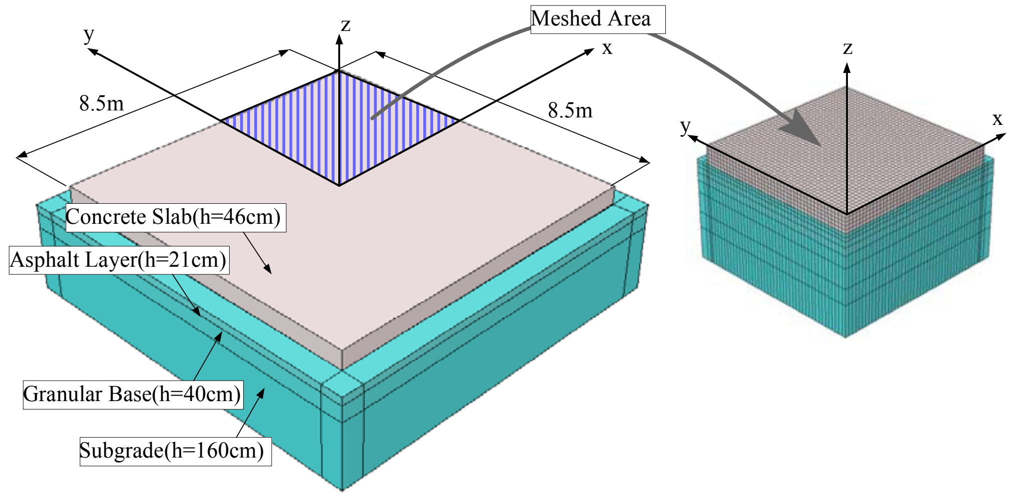

Figure 8. 3DFEM modeling of a concrete slab for thermal stress calculation

Table 3 Input parameters for material properties of the experimental pavement

Concrete Slab	Unit C	Unit D
Elastic Modulus [MPa]	39900	41700
Poisson's Ratio	0.206	0.204
Thermal Expansion Coefficient [/^{o}C]	0.00000996	0.00000892
Unit Weight [kN/m^3]	23.5	23.5
Thickness [mm]	460	460
Asphalt Layer		
Elastic Modulus [MPa]	20000	
Poisson's Ratio	0.35	
Thickness [mm]	210	
Granular Base		
Elastic Modulus [MPa]	5000	
Poisson's Ratio	0.35	
Thickness [mm]	400	
Subgrade		
Elastic Modulus [MPa]	1000	
Poisson's Ratio	0.35	
Thickness [mm]	1600	

4.3. Calculation results

Comparisons of measured and calculated restraint strain distributions throughout the slab depth are shown in Figure 11. At midnight, thermal strains are small and the computed strains are very close to the measured ones, while at daytime the calculated strains are greater than the measured ones at the top and bottom of the slab. The entire shapes of the distributions in the restraint strains are very similar between the calculated and measured ones, suggesting the validity of 3DFEM analysis. Particularly, the difference of the distributions among measuring points, 1-6, 1-4 and 1-5, is represented well by the 3DFEM simulation. Lines in the figure indicate the linear component of the strain distribution. It should be noted again that the maximum tensile strain of the linear component at the bottom of the slab is much greater than the actual strain.

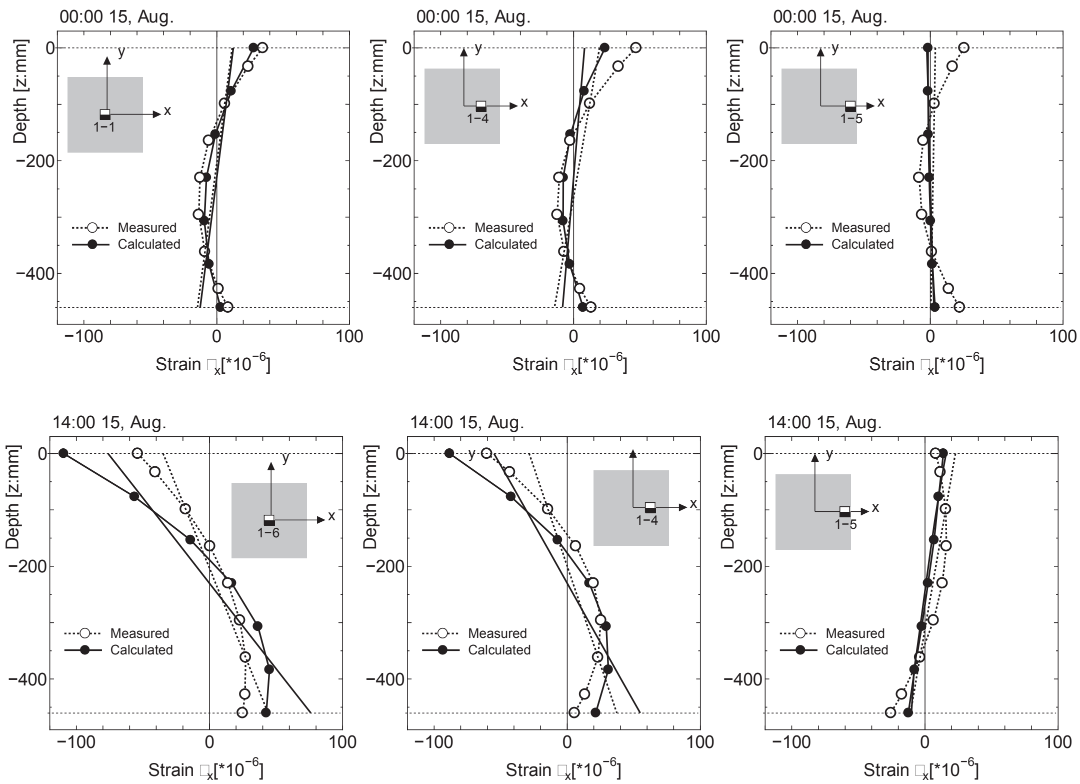

Figure 11 Comparison of measured and calculated restraint strain distributions throughout the slab depth

Comparisons of the calculated and measured thermal stress variations (solid line and dotted line, respectively) in two days in each season; October 13 to 14, January 13 to 14, April 5 to 6 and August 15 to 16 are shown in Figure 12. The measured stresses in the figure were calculated by Equation (3). Figure 12 (a) and (b) shows the thermal stress at the center of the slab. Large compressive stress is calculated at the top of the slab around 2PM when the temperature difference is the highest. The variation of the measured stress is quite similar to the calculated one. The thermal stress at the bottom of the slab is calculated in compression in night time and in tension in daytime, which is opposite to the stress at the top. The maximum stress occurs 2 hour later than the time when the maximum temperature difference takes place. The calculated maximum tensile stress is greater than the measured one in August and smaller in January. Figure 12(c) and (d) shows the thermal stress at the free edge of the slab. The stress is very small because the stress shown in the figure is the ones in the perpendicular to the direction of the slab edge and the restraint on the stress is very small. The variation of the calculated stress corresponds well with the measured one.

Figure 13 shows the same stress variations for the Unit-D. The figure is quite similar to Figure 12 and the same discussions can be made as those in Figure 12. Therefore, it can be concluded again that the thermal behavior of the high strength concrete slab is not different from the normal concrete slab.

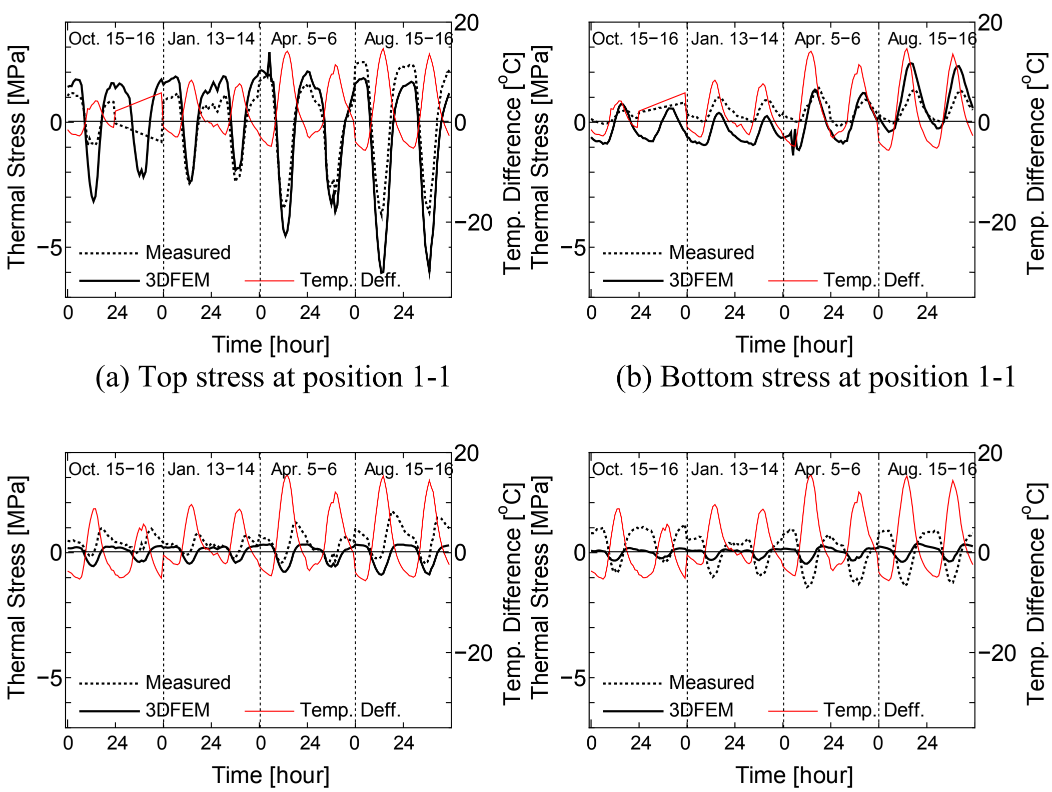

(a) Top stress at position 1-1

(b) Bottom stress at position 1-1

(c) Top stress at position 1-5

(d) Bottom stress at position 1-5

Figure 12 Comparison of thermal stress variation in time of day (Unit C)

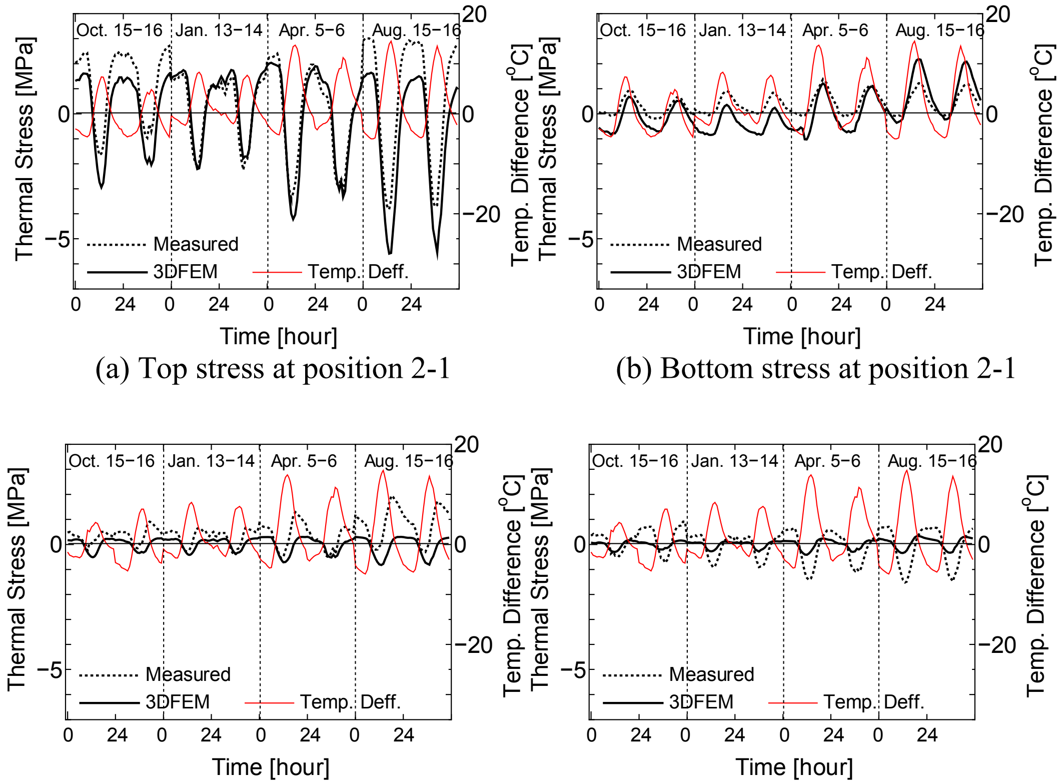

(a) Top stress at position 2-1 (b) Bottom stress at position 2-1

(c) Top stress at position 2-5 (d) Bottom stress at position 2-5

Figure 13 Comparison of thermal stress variation in time of day (Unit D)

In the structural design of airport concrete pavement, it is necessary to calculate the thermal stress at the locations anywhere aircraft loading gears pass. Since edge loading stress is generally much larger than interior loading stress, the thermal stress at slab edge should be discussed. Figure 14 shows the thermal stress distributions along the horizontal axis, *x*, which is originated at the center of the slab and increases toward the slab edge. Figure 14(a) shows the stress distributions at the top of the slab during 0AM to 6AM, Aug. 15th, when the stress is mainly in tension. Although the stress in y-direction, σy, is rather constant along the *x*-axis, σy at the edge is 20 % less than that at the center (1.75 MPa vs. 1.41 MPa). On the other hand, the stress in *x*-direction, σx, decreases significantly when the location moves from the center to the edge. The magnitude of the stress slightly changes during the period from midnight to early morning. Figure 14(b) shows the bottom stress distributions along *y*-axis during the period from 10AM to 4PM when the stress at the bottom is in tension. Again, although σy is constant along x-axis, σy is 20% less than that at the edge (2.35 MPa vs. 1.86 MPa). The magnitude of σy at the center, 2.35 MPa at the maximum, is higher than that at midnight. The magnitude of σy at the edge is 1.86 MPa at the maximum, which is the similar to the maximum top stress, 1.75 MPa, at the center at midnight. That means that the contribution of thermal stress at the edge in daytime is similar to that at the center in daytime if the loading stress is the same. σx changes drastically from in tension at the center to in compression near the edge. The stresses largely change during the period from morning to early evening.

Duration of high thermal stress of more than 2.0 MPa is short, two or three hours in a day. Accordingly, since the thermal stresses vary within a slab at each time of day, they should be estimated place by place depending on where and when aircraft gears passes. 3DFEM model is an appropriate tool to estimate the thermal stress at any place and under any thermal conditions in thick concrete slabs.

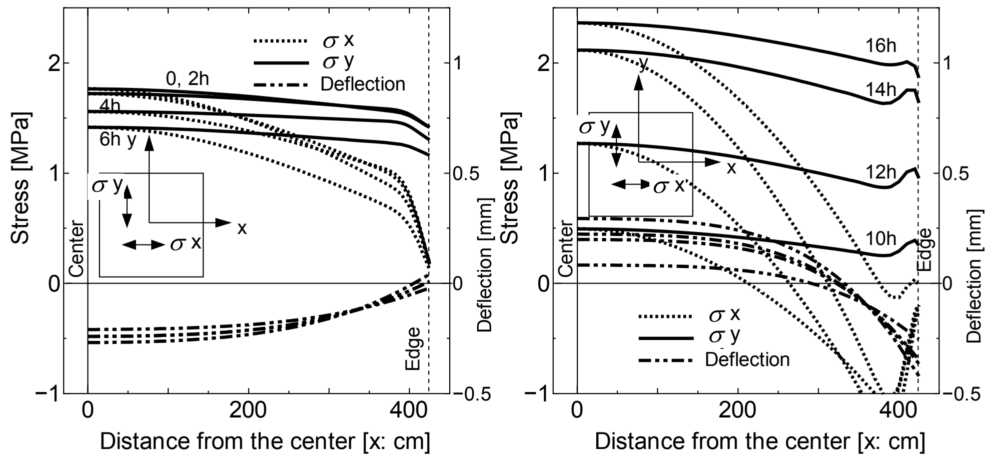

(a) Top Stress at 00:00 to 06:00 (b) Bottom Stress at 10:00 to 16:00

Figure 14. Thermal stress distributions in the slab (Aug. 15)

5. Conclusions

The thermal stresses in thick concrete slab were discussed from the strain and temperature measurements on the experimental concrete pavement with 46 thick concrete slabs. From the measurement results, the following findings were obtained:

(1) The strain and temperature distributions throughout the slab depth have a strong nonlinearity, which can be approximated well by a quadratic equation.

(2) The equation of thermal stress used in the structural design of concrete pavement in Japan overestimates the bottom stress.

(3) There is no difference in thermal stress between high strength concrete and normal concrete.

(4) Dowel bar reinforcement in joint does not affect the thermal stress near the joint.

3DFEM model was developed to estimate the thermal stresses in thick concrete slabs with a nonlinear temperature distribution throughout the slab depth. Simulations of the model revealed the followings:

(1) 3DFEM simulation provides reasonable predictions for not only thermal strain distributions throughout the slab depth at each time of day but also daily thermal stress variations in four seasons, indicating validity of the model.

(2) 3DFEM model is an appropriate tool to estimate the thermal stresses at any place at any time that are required to be estimated in the structural design procedure.

References

Choubane, B. and Tia, M. (1995) "Analysis and Verification of Thermal-Gradient Effects on Concrete Pavement", *Journal of Transportation Engineering*, ASCE, Vol.121, No.1.

Harik, I.E., Jianping, P., Southgate, H. and Allen, D. (1994) "Temperature Effects on Rigid Pavements", *Journal of Transportation Engineering*, ASCE, Vol.120, No.1.

Iwama, S. (1963) "Experimental Studies on The Structural Design of Concrete Pavement", JSCE.

Mahboub, K.C., Liu, Y., and Allen, D.L. (2004) "Evaluation of Temperature Responses in Concrete Pavement, *Journal of Transportation Engineering*, ASCE, Vol.130, No.3, pp. 395-401.

Nishizawa, T., Shimeno, S., Komatsubara, A., and Koyanagawa, M. (1998) "Study on Thermal Stresses in Continuously Reinforced Concrete Pavement", *Transportation Research Record*, No.1629, pp.99-107.

Nishizawa, T., Koyanagwa, M., Takeuchi, Y., and Kimura, M. (2005) Study on Mechanical Behavior of Dowel Bar in Transverse Joint of Concrete Pavement, *Proceedings, 7th International Conference on Concrete Pavement*.

Pane, I., Hansen, W., and Mohamed, A.R. (1998) "Three-Dimensional Finite Element Study on Effects of Nonlinear Temperature Gradients in Concrete Pavements", *Transportation Research Record*, No.1629, pp.58-65.

Shoukry, S.M., William, G.W., and Riad, M. (2003) "Nonlinear Temperature Gradient Effects in Dowel Jointed Concrete Slabs", *The International Journal of Pavement Engineering*, Vol.4, No.3, pp.131-142.

Tsubokawa, M., Mizukami, J., Hachiya, Y., and Kameda, S. (2006) "Study on Thermal Stress Due to Daily Temperature Change of Airport Concrete Pavements", *Journal of Pavement Engineering*, JSCE, pp. 157-164.

Westagaard, H.M. (1926) "Analysis of Stresses in Concete Roads Caused by Variation of Temperature", *Proceedings of the Annual Meeting*, Highway Research Board, pp. 201-215.

William, G.W., and Shoukry, S.M. (2001) "3D Finite Element Analysis of Temperature-Induced Stresses in Dowel Joint Concrete Pavements", *The International Journal of Geomechanics*, Vol. 1, No. 3, pp.291-307.